crystals

MDPI

Article

Experimental and Theoretical Studies of Carboxylic Polymers with Low Molecular Weight as Inhibitors for Calcium Carbonate Scale

Yuwei Zuo [1], Wenzhong Yang [1,*], Kegui Zhang [2,*], Yun Chen [1,*], Xiaoshuang Yin [1] and Ying Liu [1]

[1] School of Chemistry and Molecular Engineering, Nanjing Tech University, Nanjing 211816, China; 18305199218@163.com (Y.Z.); xsyin@njtech.edu.cn (X.Y.); renyuren3354@njtech.edu.cn (Y.L.)

[2] Nanjing Institute of Environmental Sciences, Ministry of Ecology and Environment of the People's Republic of China, Nanjing 210042, China

* Correspondence: yangwznjtech@163.com (W.Y.); zhangkegui@nies.org (K.Z.); ychen@njtech.edu.cn (Y.C.)

Received: 21 April 2020; Accepted: 18 May 2020; Published: 19 May 2020

Abstract: Poly acrylic acid (PAA) and polyepoxysuccinic acid (PESA) were investigated as scale inhibitors. The static experiments certified that PAA was superior to PESA for the inhibition of calcium carbonate in the low molecular weight range. The X-ray diffraction patterns suggest that the effect of PAA on the calcite (1 0 4) and (1 1 0) crystal plane was more obvious. Scanning electron microscopy was used to study the surface morphology of the depositions, which indicated that the addition of scale inhibitors could disturb the normal growth of $CaCO_3$ scale. The transmittance ratio of ferric oxide demonstrated that PAA had a better dispersion performance than PESA. The molecular dynamics simulation and quantum calculation were selected to theoretically explore the mechanism and structure of scale inhibitors, indicating that the interaction of PAA with (1 0 4) and (1 1 0) calcite crystal surfaces was stronger than PESA. In addition, the results indicated that the PAA with negative charge more easily adsorbed free Ca^{2+} in the aqueous phase. Based on these observations, PAA exhibited better scale inhibition and dispersion effects than PESA in the case of low molecular weight.

Keywords: PAA; PESA; scaling; molecular weight; calcium carbonate

1. Introduction

The main approach to alleviating the pressure on industrial water is to circulate cooling water [1,2]. However, the frequent use of circulating cooling water could inevitably result in the deposition of scale in the pipeline due to some scale-forming ions like Ca^{2+}, HCO_3^-, CO_3^-, and SO_4^{2-} [3–5]. In this case, the heat transfer efficiency of the pipeline would be detrimentally decreased [6–8]. The use of scale inhibitors is one of the effective methods to prevent the growth of scale and extend the service life of equipment [9–11].

At present, the phosphonate [12], carboxylic [13,14], sulfonic [15], and ether groups have proven to be the most effective functional groups in inhibiting crystal nucleation [16,17]. The scale inhibitors with carboxylic acid are currently used as green scale inhibitors, and the representative agents are carboxylic acid polymers [18–21]. These scale inhibitors not only have a good inhibition effect on crystalline compounds, but have also some dispersion effect [22,23]. Generally, the molecular weight has a great influence on scale inhibition [24–26]. Few studies have detailed the effect of low molecular weight (below 4000) on scale inhibition and dispersion.

In this study, two typical carboxylic polymers, poly acrylic acid (PAA) [27,28] and polyepoxysuccinic acid (PESA) [29,30], were chosen to explore the performance in inhibiting calcium carbonate scale and the inhibition mechanism. The crystal structures of calcium carbonate precipitation were examined using X-ray diffraction and the morphology features were obtained by scanning electron microscopy.

The adsorption behavior of carboxylic groups for the inhibition of calcium carbonate was exhibited at the micro level through molecular dynamics (MD) simulations [31,32]. The quantum chemical calculations [33,34] aimed to explore the mechanism of the intermolecular interactions of carboxylic groups and calcium carbonate.

2. Materials and Instruments

2.1. Materials and Instruments

Na_2CO_3 (Tianjin Chemical Importing Corporation), $NaHCO_3$ (Aklar Chemistry), sodium thiosulfate (Aklar Chemistry), potassium persulfate (Aklar Chemistry), Fe_2O_3 (Aklar Chemistry), ethyl acetate (Aklar Chemistry), and $CaCl_2{\cdot}2H_2O$ (Riedel-de Haen) were purchased from Sinopharm Chemical Reagent Co. Ltd. (Shanghai, China), all of which were of analytical reagent grade. Meanwhile, the analytical grade sodium tetraborate and tetraacetic acid disodium salt were bought from Sinopharm Chemical Reagent Co. Ltd. (China). Acrylic acid and PESA solutions were purchased from Taihe Water Treatment Co. Ltd. (Shandong, China), which comprised a 50 wt% aqueous solution. The water used in the experiment was 18.2 MΩ cm (HITECH, Medium-E400, Beijing, China)

The patterns of the $CaCO_3$ precipitations were recorded on a Bruker D8 Advance X-ray diffraction (XRD) instrument (Ettlingen, Germany), wherein the diffraction angle (2θ) was scanned in the range of 20°–70°. The dried samples of the static scale inhibition tests were obtained by filtering the mixed solutions, which were examined through scanning electron microscopy (SEM) on a SU8010 device (Tokyo, Janpan) at the acceleration voltage of 15 kV. The M_w and M_n of the inhibitors were measured by gel permeation chromatography.

2.2. Synthesis of Polyacrylic Acid

The purpose of this experiment was to synthesize low molecular weight polyacrylic acid [27,35]. First, the four-neck bottle contained deionized water and an acrylic monomer, which consisted of a mechanical agitator, a reflux condenser, a thermometer, and nitrogen. A stream of nitrogen was applied to the solution for 1 h to flush out the dissolved oxygen in the mixture. Equal amounts (wt%) of sodium thiosulfate and potassium persulfate were added to the solution while stirring (300 rpm). The nitrogen gas flow was maintained throughout the reaction. The polymer was isolated by precipitation by mixing the aqueous solution with ethyl acetate, and drying at 40–50 °C in vacuo for three days.

The characterization and molecular weights of PAA were obtained and analyzed by GPC (gel permeation chromatography, Waters, Milford, USA) to sustain the results of the synthesis.

2.3. Static Experiment

The scale inhibition performance of the selected polymers was estimated according to the Chinese National Standard (GB/T16632-2008) [36]. Experiments were carried out in a 0.5 L conical flask heated at different temperatures (30 °C and 80 °C) in a water bath for 10 h, respectively. The initial solution contained 6-mmol/L Ca^{2+} and 12-mmol/L HCO_3^-, which were adjusted to a certain value (pH = 9.0) using 0.4-mmol/L $Na_2B_4O_7$ (buffer solution). Subsequent to cooling to room temperature, the solutions were filtered through a 30-μm filter paper. Then, the concentration of Ca^{2+} was measured by EDTA titration and the scale inhibition efficiency η were obtained using the following formula [37]:

$$\eta = \frac{X_2 - X_0}{X_1 - X_0} \times 100\%, \quad (1)$$

where X_0 is the initial concentration of Ca^{2+}. X_1, X_2 represent the concentration of Ca^{2+} with and without the addition of the scale inhibitor in the test solution, respectively.

2.4. Dispersion Experiment

The dispersion characteristics of the ferrous solution at 420 nm were analyzed by a spectrometer (722 spectrophotometer, UV-1750, SHIMADZU, Kyoto, Japan) whose wavelength range was between 330–800 nm [1]. First, 150 mg/L Ca^{2+} (calcium chloride solution) and 10 mg/L (ferrous sulfate solution) were mixed in a flask. Then, different amounts of scale inhibitors were injected into the solution, and the solution's pH was adjusted to 9.0 with borax buffer solution. The solutions were stirred at room temperature for 15 min and kept in a constant temperature water bath at 50 °C for 5 h, respectively. Finally, the solution was cooled to room temperature and the supernatant taken out after constant volume. The dispersion property was evaluated by measuring the light transmittance of the ferrous solution.

2.5. Molecular Dynamics Simulation

Molecular dynamics (MD) simulations (Accelrys Inc., San Diego, CA, USA) were applied to explore the behavior between the $CaCO_3$ scales and additives, which uses the visualizer Forcite module along with a COMPASS (condensed-phase optimized molecular potential for atomistic simulation studies) forcefield [38]. Calcite belongs to the R 3(-) C space group, and the lattice parameters are listed as follows: a = b = 0.4991 nm, c = 1.7061 nm, $\alpha = \beta = 90°$, and $\gamma = 120°$ [39]. The calcite (1 0 4) and (1 1 0) crystal faces were chosen for the major research objects due to the XRD data. According to the actual experimental results, the degree of polymerization of both polymers was set to 30. All the experiments were carried out at 313 K with the NVT ensemble and Berensen method. Then, all optimized molecules were freely distributed in the box. A vacuum slab was built along the Z-axis(c) direction with thickness of 10 Å to separate the central slab and avoid the effect of additional free boundaries [40]. In addition, the $CaCO_3$ molecules at the bottom were fixed, so only the $CaCO_3$ at the top and 500 water molecules were allowed to move freely within the periodic system boundary. The non-bonding interactions were respectively computed using an atom-based and the Ewald summation method, with a cut off radius of 0.95 nm. The time step was set to 1 fs, and the MD simulation ran for 500 ps: the first 300 ps for the equilibration stage and the last 200 ps for the production stage. The interaction energy E_{inter} between the scale inhibitor and calcite was calculated using the following equation [41]:

$$E_{interaction} = E_{total} - (E_{surface} + E_{polymer}) + E_{water} \quad (2)$$

where E_{total} is the total energy of the optimized surface additive complex, and $E_{surface}$ and $E_{polymer}$ are the energy of the calcite crystal and water. E_{water} is the total energy of water. The binding energy E_b is defined as the negative value of the interaction energy:

$$E_b = -E_{inter} \quad (3)$$

2.6. Quantum Chemical Method

The quantum chemical method was performed to explore the density functional theory calculation between Ca^{2+} and the scale inhibitors. First, starting with structures in which Ca^{2+} and organic molecules were randomly arranged, they were optimized by B3LYP/6-31G (d) with density functional theory (DFT) in Gaussian 09 software (Gaussian Inc., Wallingford, CT, USA) [42,43]. Then, the final geometry and structural parameters were obtained. The frequency analysis was conducted to ensure the minimum point of the calculated structure without imaginary frequency.

3. Results and Discussion

3.1. Molecular Weight

The M_w and M_n of the inhibitors were measured by gel permeation chromatography (GPC). The weight-average molecular weight (M_w) and the number-average molecular weight (M_n) of PAA

were 6043 g/mol and 3798 g/mol, respectively. As a reference, the values of PESA were 4119 g/mol and 2541 g/mol, respectively. These results indicate that the measured values were within the range required [44].

3.2. Static Scale Inhibition Analysis

As shown in Figure 1, the relationship between the concentration of scale inhibitors and the ability to inhibit the calcium carbonate scale was investigated [45]. Meanwhile, considering the effect of temperature on the scale inhibition efficiency, two temperatures of 30 °C and 80 °C were selected for the experimental research. The scale inhibition efficiency reached 90% and 95% for PESA and PAA at 3.33 μM, respectively. Notably, the inhibition efficiency of PAA increased more rapidly, which showed that it was better at inhibiting the calcium carbonate in water. Interestingly, both scale inhibitors were affected at high temperature. Curiously, the inhibition efficiency of both additives at 80 °C at the same concentration range was similar. Thus, the inhibition efficiencies by both polymers seem to be correlated with the type of polymorph precipitated.

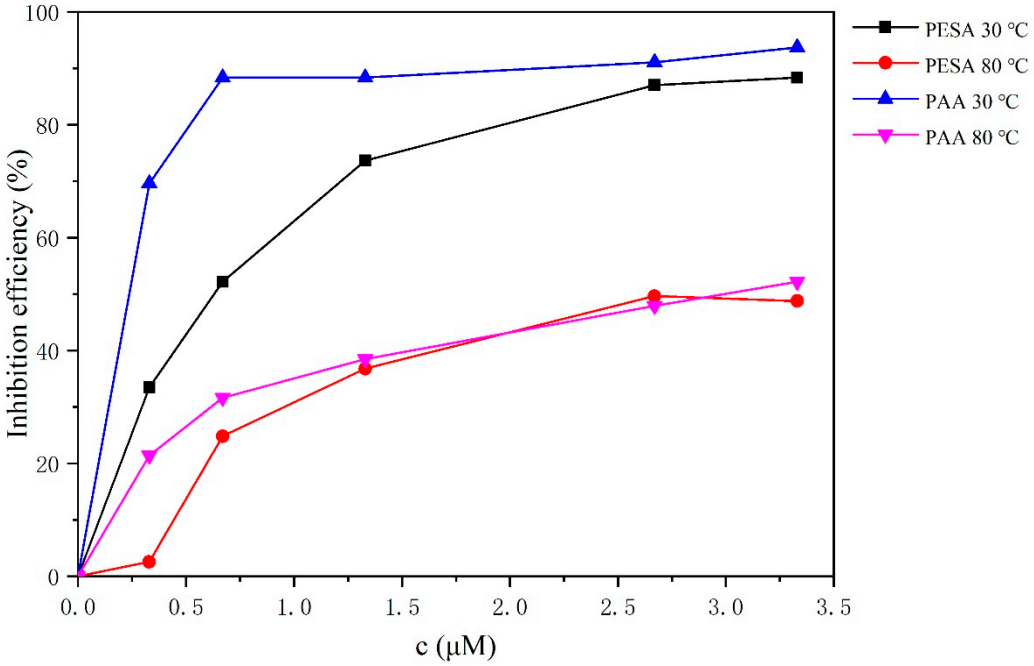

Figure 1. The inhibition efficiency of the two inhibitors at 30 °C and 80 °C.

To prove the effect of different scale inhibitors on the crystal structure of calcium carbonate, the transformation was identified using XRD. The results of XRD for precipitates with different concentrations of inhibitors at 30 °C and 80 °C are presented in Figure 2. What was observed was a similar tendency in the precipitation of the polymorphs of calcium carbonate, but at different concentrations of both inhibitors in the crystallization media. As presented in Figure 2, the crystal structure was in the form of calcite in the absence of PESA and PAA. With the addition of a low concentration of two scale inhibitors, what happens is that PAA and PESA are efficient in favoring the metastable polymorphs aragonite and vaterite in different concentration ranges of the additive. In the high concentration range, a higher concentration or equal to 1.33 μM, is more effective in favoring vaterite at 30 °C, while at 80 °C, the behavior of both additives was more similar. For PAA, it was obvious that vaterite was favored more quickly at 30 °C than at 80 °C, which was the same for PESA. This indicates that the crystal structure of calcium carbonate is influenced by different temperatures. It is obvious that the inhibition effect of PESA and PAA on the surface of (1 0 4) ($2\theta = 29.45°$) and (1 1 0) ($2\theta = 35.96°$) was more effective than that on other surfaces of calcite. The XRD analysis also confirmed

that the form of the $CaCO_3$ deposit changed from the more stable calcite crystal to the unstable vaterite in the presence of PESA and PAA.

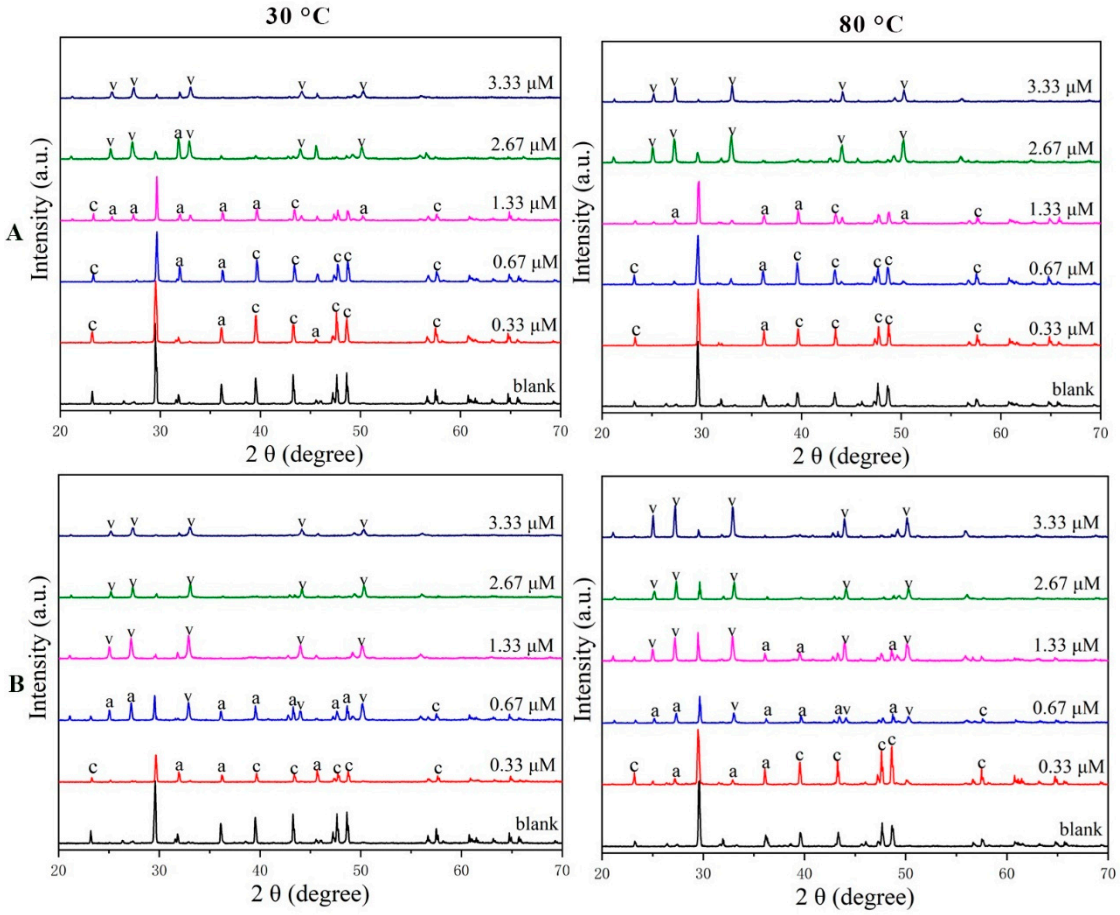

Figure 2. The X-ray diffraction (XRD) results for the depositions with different concentrations of (**A**) polyepoxysuccinic acid (PESA), (**B**) poly acrylic acid (PAA) at 30 °C, and 80 °C. c, a, and v represent calcite, aragonite, and vaterite, respectively.

Figure 3 presents the SEM images of $CaCO_3$ in the absence and presence of different concentrations of the examined scaling inhibitors. The crystal structures of $CaCO_3$ displayed regular rhombohedral shapes in the absence of PESA and PAA. Due to the addition of the concentration of 0.67 μM of the scale inhibitors, the crystal started to become loose and porous. Furthermore, Figure 3C shows that the $CaCO_3$ precipitate transformed into an irregular sphere with a sheet structure when the concentration of the scale inhibitors reached 3.33 μM. Simultaneously, with the addition of the scale inhibitor, the crystal morphology and size of the calcium carbonate were remarkably changed. In particular, the crystals were more dispersed and had smaller sizes in the presence of PAA.

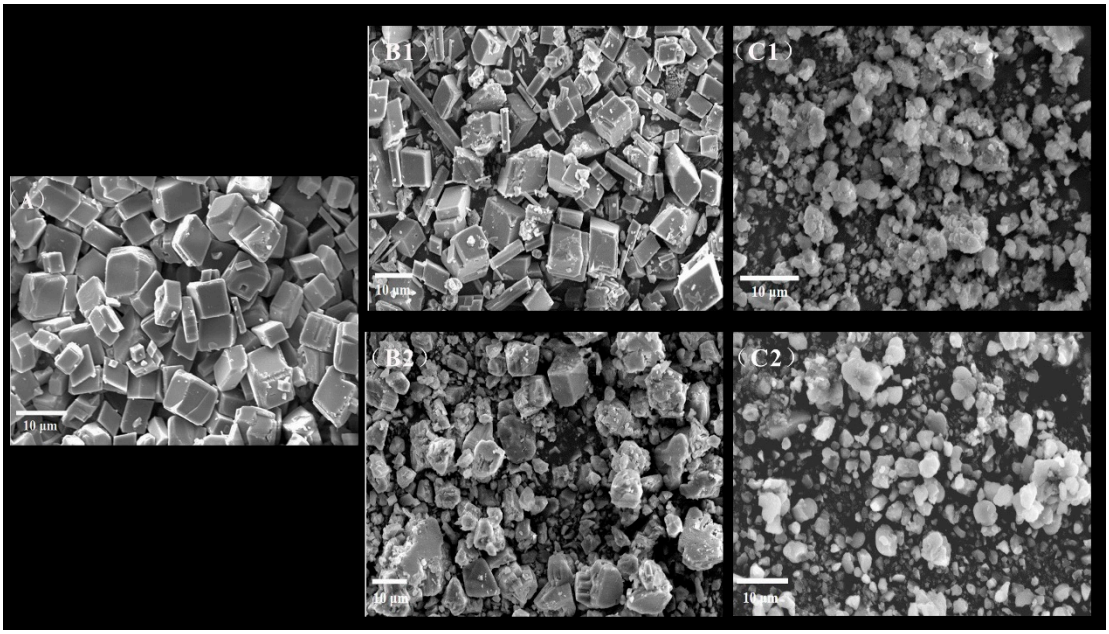

Figure 3. The scanning electron microscopy (SEM) images of $CaCO_3$ in the absence and presence of PESA and PAA at 80 °C. (**A**) blank, (**B1**,**B2**) (**C1**,**C2**) had 0.67 and 3.33 μM PESA and PAA, respectively.

It was found that both polymers had a certain dispersion effect based on the SEM data. Figure 4 reveals the dispersion capacity of the inhibitors for ferric oxide. Obviously, the transmittance ratio decreased with the increasing concentration of the inhibitors [1]. As shown in Figure 4, the order of the transmittance ratio at the same concentration was PAA > PESA. For PESA, it showed a worse dispersion performance and the transmittance ratio decreased from 95.69% to 36.215% with the concentration increasing from 0.33 mg/L to 3.33 mg/L. PAA showed a better dispersion performance, wherein its transmittance ratio decreased from 69.67% to 29.63%, which indicates that PAA has a better dispersion performance than PESA within this molecular weight range.

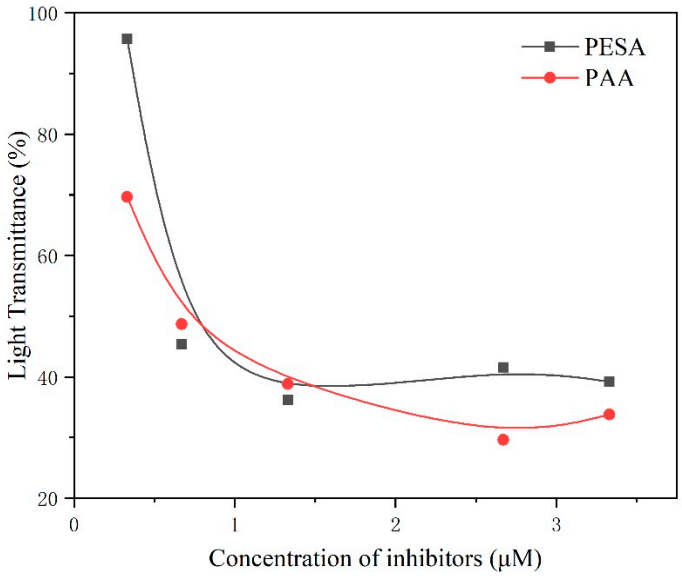

Figure 4. Effect of the PESA and PAA on the dispersion of ferric oxide at different concentrations.

3.3. Analysis of Theoretical Calculations

Molecular simulation software was used to simulate the interaction between calcium carbonate crystals and additives under the compass force field. The XRD data revealed that the (1 0 4) and (1 1 0) crystal surfaces of calcite were two obvious acting planes. To verify whether the system reached equilibrium, the fluctuation range of energy and temperature should be confined to 5–10% [46]. In the last 100 ps of the equilibrium period, the temperature and energy fluctuation curves in the molecular dynamics simulations of the two scale inhibitors on the surface of the $CaCO_3$ crystals (1 0 4) and (1 1 0) are shown in Figure 5. The system was found to be in equilibrium by observation, which indicates that the subsequent analysis results were reliable. As presented in Figure 6, the organic molecules established contact with the outermost layer of the calcite crystal. Moreover, the carboxyl groups of the organic molecules were closest to the crystal surface, overcoming the steric effect.

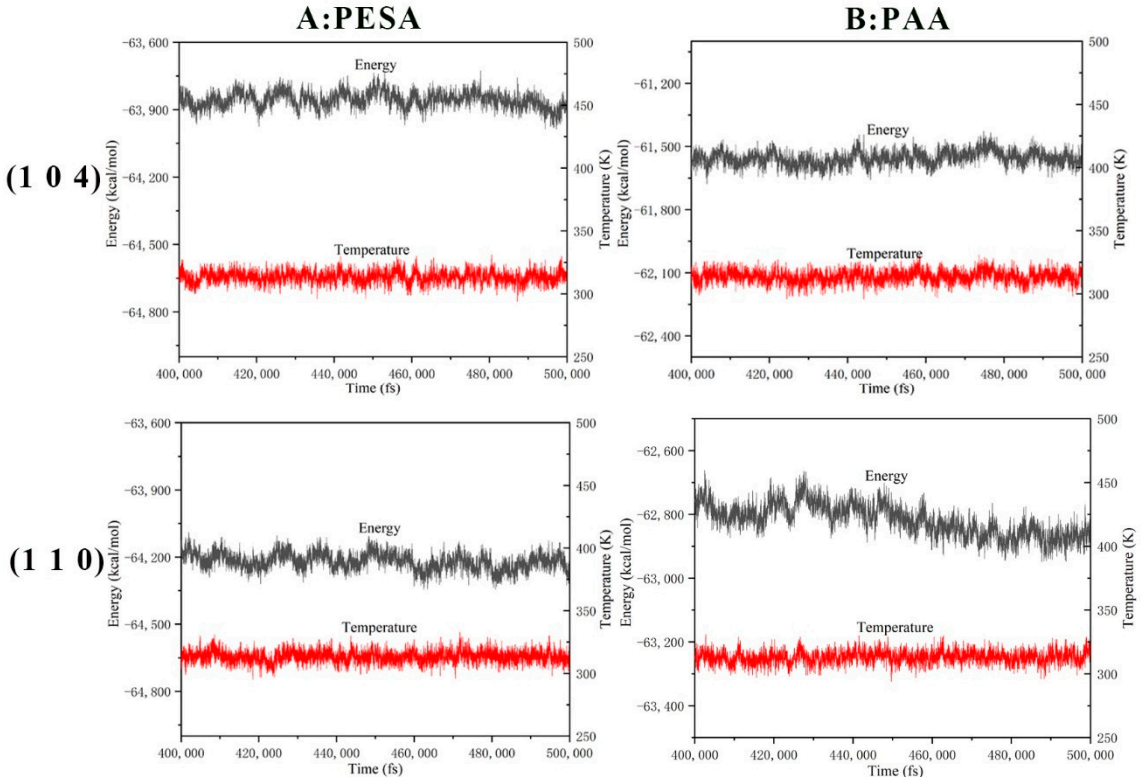

Figure 5. Fluctuations of energy and temperature during the final 100 ps of molecular simulation, (**A**) PESA; (**B**) PAA.

The interaction energies and the binding energies of both scale inhibitors and calcite systems are shown in Table 1. The positive binding energies show that the combination of the organic materials with calcite crystal surfaces are a stable phenomenon, and the more positive values suggest higher inhibition efficiencies [46,47]. The binding energy of the two polymers with the calcite (1 1 0) plane is high, which implies the ability of both to prevent the growth of the calcite crystal surface. The binding energies for PESA were 69.698 kcal/mol and 86.212 kcal/mol of calcite for the (1 0 4) and (1 1 0) surfaces, respectively. For PAA, the binding energies of the two calcite crystal faces were 106.229 kcal/mol and 141.308 kcal/mol, respectively. In comparison, it was found that the effect of PAA on calcite was more effective than PESA. These consequences are consistent with the conclusions of static scale inhibition experiments, which demonstrated that PAA had a better inhibition efficiency.

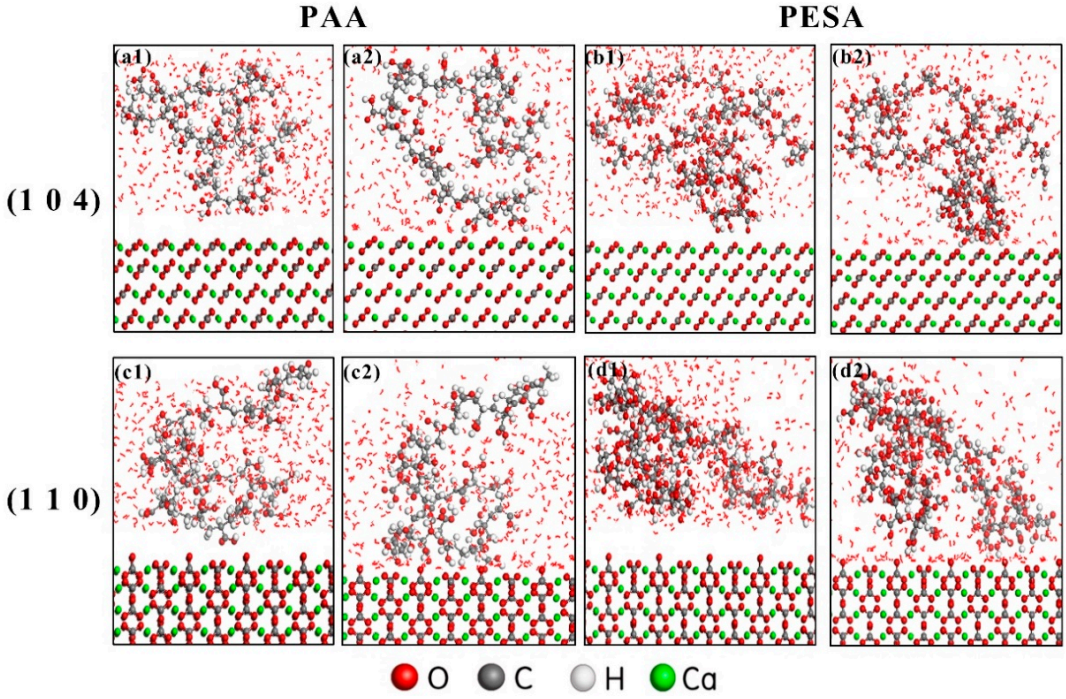

Figure 6. The initial configurations and the optimized results of the two inhibitors on the surfaces of the calcite. For PAA, (**a1**,**c1**) represent the starting configurations on the (1 0 4) and (1 1 0) faces, respectively, while (**a2**,**c2**) are the optimized simulation results correspondingly; for PESA, (**b1**,**d1**) display the starting configurations on the investigated faces and the homologous optimal simulation results are shown in (**b2**,**d2**).

Table 1. The interaction energy (kcal/mol) of the two compounds with calcite (1 0 4) and (1 1 0) surfaces.

Surfaces	Molecules	E_{inter}	E_b
(1 0 4)	PESA	−69.698	69.698
	PAA	−106.229	106.229
(1 1 0)	PESA	−86.212	86.212
	PAA	−141.308	141.308

Both polymers were optimized using the B3LYP-6-31G (d) method and the optimal minimum energy values of the structures are shown in Figures 7 and 8. From the negative charge value obtained in Table 2, they were mainly distributed on the O atoms of the carboxylic acid group of polymers. Negatively charged atoms will be associated with Ca^{2+} on the surface due to the electrostatic interaction. The Coulomb interaction energy (F) is dependent on the distance (r) and charges (q) as per the following equation:

$$F = \sum_{i<j}^{n} \frac{q_i q_j}{4\pi\varepsilon {r_{ij}}^2} \quad (4)$$

where ε is the dielectric constant; q_i represents the calcium ion; and q_j represents the negative charge of the atoms in inhibitor molecules. $F < 0$ indicates an electrostatic attractive force, while $F > 0$ represents an electrostatic repulsive force.

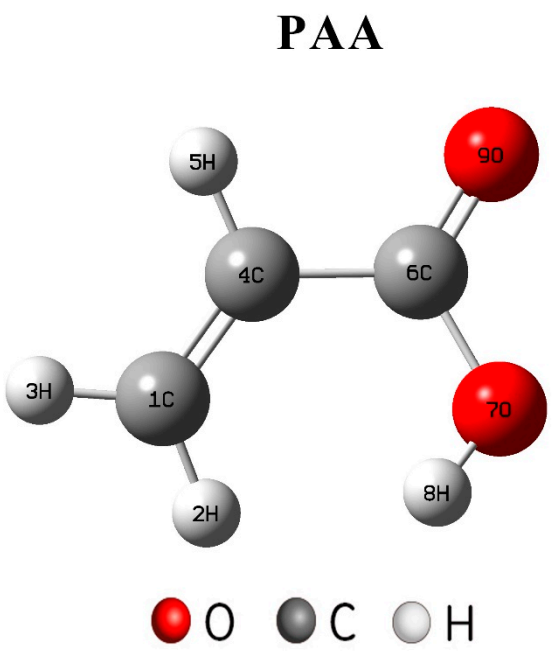

Figure 7. Optimal configurations of PAA.

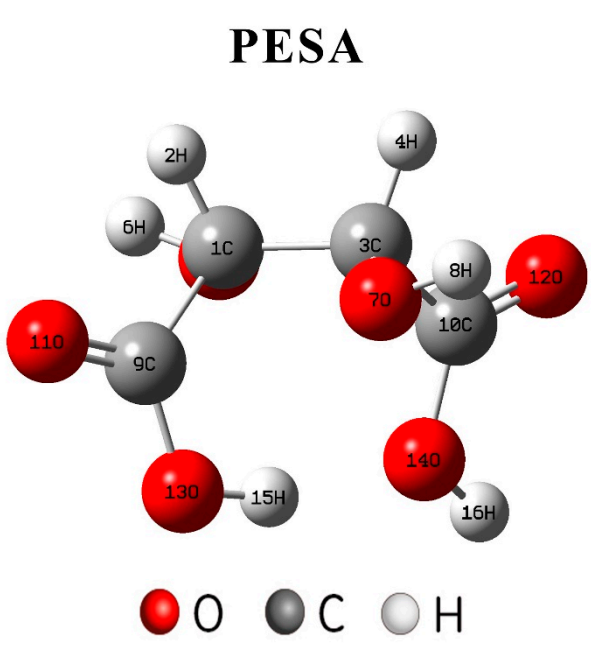

Figure 8. Optimal configurations of PESA.

Table 2. Negative charge distribution of two molecules.

Inhibitors	O(–H)	(C=)O
PESA	−0.554	−0.389
PAA	−0.610	−0.438

As listed in Table 2, the oxygen atoms of the carboxylic acid moieties of PESA and PAA exhibit negative charges, which are able to adsorb Ca^{2+}. Furthermore, the amount of negative charge is the key to affect the capacity of electrostatic interaction [48]. The more negative the charge, the easier it is to adsorb calcium ions. Hence, the carboxylic groups of PAA have more negative charge, which is more likely to interact with calcium ions.

3.4. Scaling Inhibition Mechanism

In this study, PAA displayed better scale inhibition efficiency and dispersion effect than PESA. As shown in Figure 9, the SEM data demonstrated that PAA could induce a lattice distortion of calcium carbonate crystals from calcite to vaterite formation. The inhibition efficiency and dispersion capacity were completed in the dissolved state. Subsequent to the addition of the scale inhibition, it tends to be adsorbed on the nucleus of the calcium carbonate crystal during the scale formation process. Due to the occupation of the active growth position, inhibitors hinder the normal growth of the crystal and changes the lattice parameter, which shows the inhibition of scale formation. At the same dosage, PAA contains more carboxylic acid groups, which leads to a better scale inhibition efficiency than PESA. The organic carboxylic scale inhibitor is relatively large in molecular size and is easy to wrap around the generated small particles, which controls the growth of small particles. Moreover, PAA dissociates into anions in an aqueous solution that can adhere to calcium carbonate through electrostatic interactions to achieve dispersion and stabilization effects of inorganic scale. Hence, PAA with more negative charges is shown to effectively chelate with free Ca^{2+} ions in the aqueous phase. Meanwhile, the chelation power of PAA with respect to Ca^{2+} is higher than that of PESA, which shows that PAA has a better scale inhibition performance.

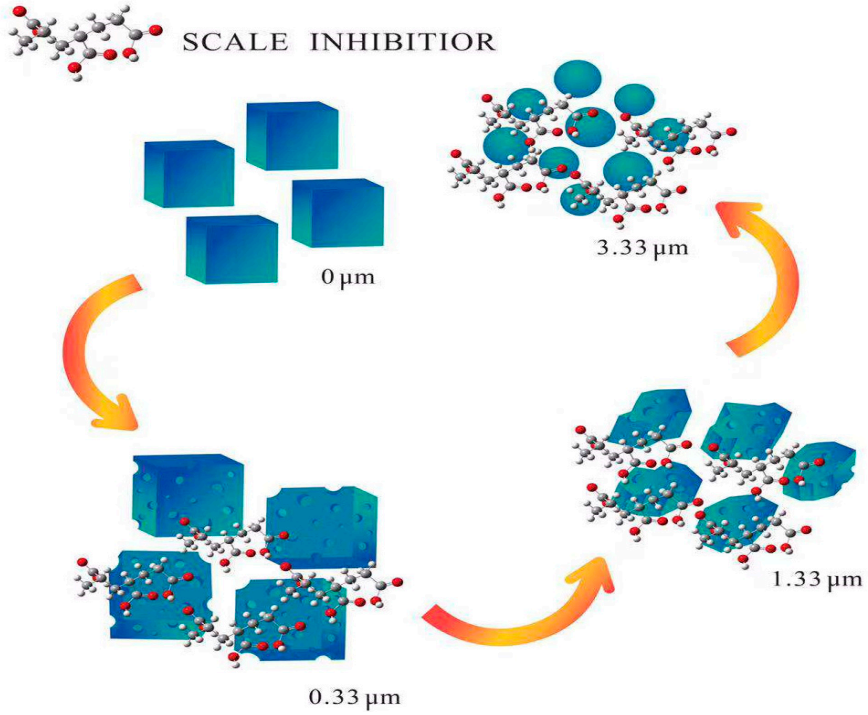

Figure 9. Schematic illustration of the mechanism.

4. Conclusions

In this study, the key conclusions can be summarized as follows:

1. The static experiments revealed that at normal temperatures, PAA exhibited a better inhibition performance than PESA at low molecular weights, while in elevated temperatures, the behavior of both additives was more similar.
2. PAA was demonstrated to exhibit better dispersion performance than PESA within this investigated molecular weight range.
3. Results of the XRD and SEM revealed that PAA and PESA inhibited the growth of the calcite phase at the (1 0 4) and (1 1 0) crystal planes, and favored the nucleation of vaterite.

4. The stronger binding energies of PAA rendered the interaction of PAA with (1 0 4) and (1 1 0) calcite crystal surfaces stronger than that of PESA.
5. Due to the different number of free carboxylic groups of PAA and PESA, PAA had more carboxylic acid groups, which led to a better scale inhibition efficiency than that of PESA.

Author Contributions: Conceptualization, W.Y.; Data curation, Y.Z.; Formal analysis, Y.Z.; Funding acquisition, W.Y.; Investigation, Y.Z.; Methodology, Y.Z.; Project administration, X.Y., Y.C., Y.L. and K.Z.; Supervision, W.Y.; Visualization, K.Z.; Writing—original draft, Y.Z.; Writing—review and editing, Y.Z. All authors have read and agreed to the published version of the manuscript.

Funding: Financial support from the National Key R&D Plan (2017YFC0404100), the National Natural Science Foundation of China (21605084), and the Project supported by the Natural Science Foundation for Young Scholars of Jiangsu Province, China (Grant No. BK20160983) are highly appreciated.

Conflicts of Interest: The authors declare no conflict of interest.

References

1. Yang, L.; Yang, W.; Xu, B.; Yin, X.; Chen, Y.; Liu, Y.; Ji, Y.; Huan, Y. Synthesis and scale inhibition performance of a novel environmental friendly and hydrophilic terpolymer inhibitor. *Desalination* **2017**, *416*, 166–174. [CrossRef]
2. Zhao, Y.; Xu, Z.; Wang, B.; He, J. Scale inhibition performance of sodium carboxymethyl cellulose on heat transfer surface at various temperatures: Experiments and molecular dynamics simulation. *Int. J. Heat Mass Transf.* **2019**, *141*, 457–463. [CrossRef]
3. Okumura, M.; Kitano, Y. Coprecipitation of alkali metal ions with calcium carbonate. *Geochimica et Cosmochimica Acta* **1986**, *50*, 49–58. [CrossRef]
4. Liu, G.; Xue, M.; Yang, H. Polyether copolymer as an environmentally friendly scale and corrosion inhibitor in seawater. *Desalination* **2017**, *419*, 133–140. [CrossRef]
5. Zhang, S.; Qu, H.; Yang, Z.; Fu, C.-E.; Tian, Z.; Yang, W. Scale inhibition performance and mechanism of sulfamic/amino acids modified polyaspartic acid against calcium sulfate. *Desalination* **2017**, *419*, 152–159. [CrossRef]
6. Shen, C.; Xu, X.; Hou, X.-Y.; Wu, D.-X.; Yin, J.-H. Molecular weight effect on PAA antiscale performance in LT-MED desalination system: Static experiment and MD simulation. *Desalination* **2018**, *445*, 1–5. [CrossRef]
7. Yu, W.; Wang, Y.; Li, A.; Yang, H. Evaluation of the structural morphology of starch-graft-poly(acrylic acid) on its scale-inhibition efficiency. *Water Res.* **2018**, *141*, 86–95. [CrossRef]
8. Zheng, T.; Zhang, X.; Yi, H. Spherical vaterite microspheres of calcium carbonate synthesized with poly (acrylic acid) and sodium dodecyl benzene sulfonate. *J. Cryst. Growth* **2019**, *528*, 125275. [CrossRef]
9. Reddy, M.M.; Hoch, A.R. Calcite Crystal Growth Rate Inhibition by Polycarboxylic Acids. *J. Colloid Interface Sci.* **2001**, *235*, 365–370. [CrossRef]
10. Chauhan, K.; Kumar, R.; Kumar, M.; Sharma, P.; Chauhan, G.S. Modified pectin-based polymers as green antiscalants for calcium sulfate scale inhibition. *Desalination* **2012**, *305*, 31–37. [CrossRef]
11. Chen, J.; Xu, L.; Han, J.; Su, M.; Wu, Q. Synthesis of modified polyaspartic acid and evaluation of its scale inhibition and dispersion capacity. *Desalination* **2015**, *358*, 42–48. [CrossRef]
12. Ji, Y.; Chen, Y.; Le, J.; Qian, M.; Huan, Y.; Yang, W.; Yin, X.; Liu, Y.; Wang, X.; Chen, Y. Highly effective scale inhibition performance of amino trimethylenephosphonic acid on calcium carbonate. *Desalination* **2017**, *422*, 165–173. [CrossRef]
13. Zhao, Y.; Jia, L.; Liu, K.; Gao, P.; Ge, H.; Fu, L. Inhibition of calcium sulfate scale by poly (citric acid). *Desalination* **2016**, *392*, 1–7. [CrossRef]
14. Abdel-Aal, N.; Sawada, K. Inhibition of adhesion and precipitation of $CaCO_3$ by aminopolyphosphonate. *J. Cryst. Growth* **2003**, *256*, 188–200. [CrossRef]
15. Mady, M.F.; Malmin, H.; Kelland, M.A. Sulfonated Nonpolymeric Aminophosphonate Scale Inhibitors—Improving the Compatibility and Biodegradability. *Energy Fuels* **2019**, *33*, 6197–6204. [CrossRef]
16. Zhang, H.-P.; Luo, X.-G.; Lin, X.-Y.; Tang, P.-P.; Lu, X.; Yang, M.-J.; Tang, Y. Biodegradable carboxymethyl inulin as a scale inhibitor for calcite crystal growth: Molecular level understanding. *Desalination* **2016**, *381*, 1–7. [CrossRef]

17. Menzri, R.; Ghizellaoui, S.; Tlili, M. Calcium carbonate inhibition by green inhibitors: Thiamine and Pyridoxine. *Desalination* **2017**, *404*, 147–154. [CrossRef]
18. Zhang, W.; Gongwei, L.; Jin, F.; Huo, Y.; Sun, T.; Li, C. Synthesis and characterization of an ionic liquid-carboxylic acid copolymer scale inhibitor and its scale inhibition performance. *Water Supply* **2019**, *19*, 1463–1472. [CrossRef]
19. Liu, D.; Dong, W.; Li, F.; Hui, F.; Lédion, J. Comparative performance of polyepoxysuccinic acid and polyaspartic acid on scaling inhibition by static and rapid controlled precipitation methods. *Desalination* **2012**, *304*, 1–10. [CrossRef]
20. Sonobe, Y.; Watamura, H.; Hirasawa, I. Polymorphism, Size and Shape Control of Calcium Carbonate Crystals in the Presence of a Polyelectrolyte. *Chem. Eng. Technol.* **2015**, *38*, 1053–1058. [CrossRef]
21. Rabizadeh, T.; Morgan, D.J.; Peacock, C.L.; Benning, L.G. Effectiveness of Green Additives vs Poly(acrylic acid) in Inhibiting Calcium Sulfate Dihydrate Crystallization. *Ind. Eng. Chem. Res.* **2019**, *58*, 1561–1569. [CrossRef]
22. Al-Hamzah, A.A.; East, C.P.; Doherty, W.O.S.; Fellows, C.M. Inhibition of homogenous formation of calcium carbonate by poly (acrylic acid). The effect of molar mass and end-group functionality. *Desalination* **2014**, *338*, 93–105. [CrossRef]
23. Laukala, T.; Kronlund, D.; Heiskanen, I.; Backfolk, K. The effect of polyacrylic acid and reaction conditions on nanocluster formation of precipitated calcium carbonate on microcellulose. *Cellulose* **2017**, *88*, 2409–2826. [CrossRef]
24. Doherty, W.; Fellows, C.; Gorjian, S.; Senogles, E.; Cheung, A. Inhibition of calcium oxalate monohydrate by poly(acrylic acid)s with different end groups. *J. Appl. Polym. Sci.* **2003**, *91*, 2035–2041. [CrossRef]
25. Rehman, A.U.; Khan, A.; Humayun, M.; Bibi, G.; Shi, K.; Raziq, F. Effect of biocides and anionic homopolymeric inhibitors on the precipitation behavior of calcium fluoride. *Bull. Chem. Soc. Ethiop.* **2017**, *31*, 115. [CrossRef]
26. Köken, N. Polymers containing amino bis(methylene phosphonic acid) groups for scale inhibition. *Pigment Resin Technol.* **2019**, *48*, 73–83. [CrossRef]
27. Moulay, S.; Boukherissa, M.; Abdoune, F.; Benabdelmoumene, F. Low Molecular Weight Poly(acrylic acid) as a Salt Scaling Inhibitor in Oilfield Operations. *J. Iran. Chem. Soc.* **2005**, *2*, 212–219. [CrossRef]
28. Alhamzah, A.; Smith, E.; Fellows, C. Inhibition of Homogeneous Formation of Magnesium Hydroxide by Low Molar Mass Poly(Acrylic Acid) with Different End-Groups. *Ind. Eng. Chem. Res.* **2015**, *54*, 150203192126006.
29. Shi, W.-Y.; Ding, C.; Yan, J.-L.; Han, X.-Y.; Lv, Z.-M.; Lei, W.; Xia, M.-Z.; Wang, F.-Y. Molecular dynamics simulation for interaction of PESA and acrylic copolymers with calcite crystal surfaces. *Desalination* **2012**, *291*, 8–14. [CrossRef]
30. Zhang, B.; Sun, P.; Chen, F.; Li, F. Synergistic inhibition effect of polyaminoamide dendrimers and polyepoxysuccinic acid on silica polymerization. *Colloids Surf. A Physicochem. Eng. Asp.* **2012**, *410*, 159–169. [CrossRef]
31. Zhu, B.; Xu, X.; Tang, R. Hydration layer structures on calcite facets and their roles in selective adsorptions of biomolecules: A molecular dynamics study. *J. Chem. Phys.* **2013**, *139*, 234705. [CrossRef] [PubMed]
32. Yuan, P.-Q.; Cheng, Z.-M.; Zhou, Z.-M.; Yuan, W.-K.; Semiat, R. Zeta potential on the anti-scalant modified sub-micro calcite surface. *Colloids Surf. A Physicochem. Eng. Asp.* **2008**, *328*, 60–66. [CrossRef]
33. Prabhakar, S.; Melnik, R. Influence of Mg2+, SO42− and Na+ ions of sea water in crude oil recovery: DFT and ab initio molecular dynamics simulations. *Colloids Surf. A Physicochem. Eng. Asp.* **2018**, *539*, 53–58. [CrossRef]
34. Zhang, R.; Wang, X.; Zhou, L.; Liu, Z.; Crump, D. The impact of dissolved oxygen on sulfate radical-induced oxidation of organic micro-pollutants: A theoretical study. *Water Res.* **2018**, *135*, 144–154. [CrossRef] [PubMed]
35. Kavitha, A.L.; Vasudevan, T.; Prabu, H.G. Evaluation of synthesized antiscalants for cooling water system application. *Desalination* **2011**, *268*, 38–45. [CrossRef]
36. Yuan, X.; Dong, S.; Zheng, Q.; Yang, W.; Huang, T. Novel and efficient curcumin based fluorescent polymer for scale and corrosion inhibition. *Chem. Eng. J.* **2020**, *389*, 124296. [CrossRef]
37. Suo, G.; Xie, L.; Xu, S.; Feng, L.; Dong, T.; Shao, X. Study on inhibitors' performance under the condition of high concentration ratio in MED system. *Desalination* **2018**, *437*, 100–107. [CrossRef]

38. Ylikantola, A.; Linnanto, J.; Knuutinen, J.; Oravilahti, A.; Toivakka, M. Molecular modeling studies of interactions between sodium polyacrylate polymer and calcite surface. *Appl. Surf. Sci.* **2013**, *276*, 43–52. [CrossRef]
39. Chen, C.; Lei, W.; Xia, M.; Wang, F.; Gong, X. Molecular modeling of several phosphonates onto the stepped calcite (0 1 1) surface. *Desalination* **2013**, *309*, 208–212. [CrossRef]
40. Liu, Q.; Wang, Q.; Xiang, L. Influence of poly acrylic acid on the dispersion of calcite nano-particles. *Appl. Surf. Sci.* **2008**, *254*, 7104–7108. [CrossRef]
41. Shi, W.; Xia, M.; Lei, W.; Wang, F. Molecular dynamics study of polyether polyamino methylene phosphonates as an inhibitor of anhydrite crystal. *Desalination* **2013**, *322*, 137–143. [CrossRef]
42. Dubis, A.; Zamaraeva, M.V.; Siergiejczyk, L.; Charishnikova, O.; Shlyonsky, V. Ferutinin as a Ca(2+) complexone: Lipid bilayers, conductometry, FT-IR, NMR studies and DFT-B3LYP calculations. *Dalton Trans.* **2015**, *44*, 16506–16515. [CrossRef] [PubMed]
43. Wang, L.; Yang, F.; Zhao, X.; Li, Y. Effects of nitro- and amino-group on the antioxidant activity of genistein: A theoretical study. *Food Chem.* **2019**, *275*, 339–345. [CrossRef]
44. Zhang, K.; Yang, W.; Xu, B.; Chen, Y.; Yin, X.; Liu, Y.; Zuo, H. Inhibitory effect of konjac glucomanan on pitting corrosion of AA5052 aluminium alloy in NaCl solution. *J. Colloid Interface Sci.* **2018**, *517*, 52–60. [CrossRef] [PubMed]
45. Elliot, M.N. Scale control by threshold treatment. *Desalination* **1970**, *8*, 221–236. [CrossRef]
46. Zhang, K.; Xu, B.; Yang, W.; Yin, X.; Liu, Y.; Chen, Y. Halogen-substituted imidazoline derivatives as corrosion inhibitors for mild steel in hydrochloric acid solution. *Corros. Sci.* **2015**, *90*, 284–295. [CrossRef]
47. Tang, Y.; Yang, X.; Yang, W.; Wan, R.; Chen, Y.; Yin, X. A preliminary investigation of corrosion inhibition of mild steel in 0.5M H2SO4 by 2-amino-5-(n-pyridyl)-1,3,4-thiadiazole: Polarization, EIS and molecular dynamics simulations. *Corros. Sci.* **2010**, *52*, 1801–1808. [CrossRef]
48. Weber, E.; Levy, D.; Sasson, M.B.; Fitch, A.N.; Pokroy, B. Structural analysis of metal-doped calcium oxalate. *RSC Adv.* **2015**, *5*, 98626–98633. [CrossRef]